Inorganic Chemistry

Article

pubs.acs.org/IC

Thermodynamics of Axial Substitution and Kinetics of Reactions with Amino Acids for the Paddlewheel Complex Tetrakis(acetato)chloridodiruthenium(II,III)

Rodrigo L. S. R. Santos,[†,‡] Rudi van Eldik,*[,‡] and Denise de Oliveira Silva*[,†]

[†]Departamento de Química Fundamental, Instituto de Química, Universidade de São Paulo, Av. Prof. Lineu Prestes, 748, CEP 05508-000, São Paulo, SP, Brazil

[‡]Inorganic Chemistry, Department of Chemistry and Pharmacy, University of Erlangen-Nuremberg, Egerlandstr. 1, 91058 Erlangen, Germany

Supporting Information

ABSTRACT: The known paddlewheel, tetrakis(acetato)-chloridodiruthenium(II,III), offers a versatile synthetic route to a novel class of antitumor diruthenium(II,III) metallo drugs, where the equatorial ligands are nonsteroidal anti-inflammatory carboxylates. This complex was studied here as a soluble starting prototype model for antitumor analogues to elucidate the reactivity of the $[Ru_2(CH_3COO)_4]^+$ framework. Thermodynamic studies on equilibration reactions for axial substitution of water by chloride and kinetic studies on reactions of the diaqua complexes with the amino acids glycine, cysteine, histidine, and tryptophan were performed. The standard thermodynamic reaction parameters $\Delta H°$, $\Delta S°$, and $\Delta V°$ were determined and showed that both of the sequential axial substitution reactions are enthalpy driven. Kinetic rate laws and rate constants were determined for the axial substitution reactions of coordinated water by the amino acids that gave the corresponding aqua(amino acid)−Ru_2 substituted species. The results revealed that the $[Ru_2(CH_3COO)_4]^+$ paddlewheel framework remained stable during the axial ligand substitution reactions and was also mostly preserved in the presence of the amino acids.

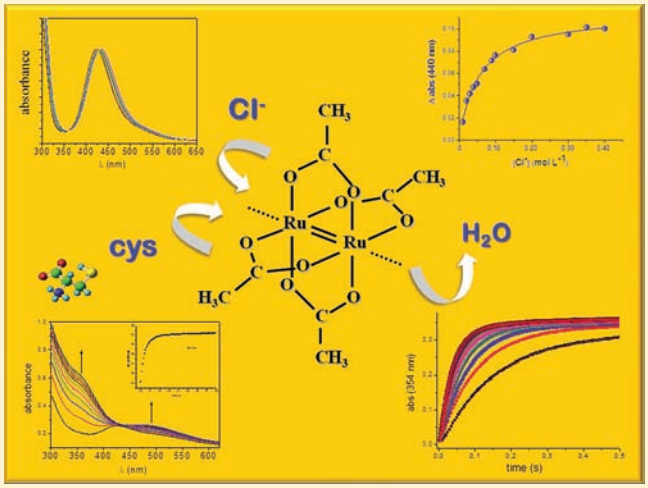

Metal−metal multiple bonded tetracarboxylates of the form $[Ru_2(RCOO)_4(L)_x]^{n+}$ (L = Lewis base or anion, x = 0, 1, 2) have sparked growing interest in both theoretical and experimental fields during the last years.[1] These compounds typically adopt a paddlewheel geometry in which each carboxylate bridges two metal atoms in equatorial positions and the ligand L occupies the axial positions. The first syntheses were reported in 1966,[2] and insight into the structures was gained in 1969 when the crystal structure of $[Ru_2(C_4H_7COO)_4Cl]$ was published by Cotton and co-workers,[3] providing the first evidence for a strong Ru−Ru bond with a bond order of 2.5 and a short bond distance of 2.281(4) Å. The $[Ru_2(RCOO)_4]^+$ paddlewheel complexes have a Ru_2(II,III) mixed-valence core (better represented by $[Ru_2]^{5+}$ since the two metal centers have been found to be equivalent) and a $\sigma^2\pi^4\delta^2$ $(\delta^*\pi^*)^3$ ground state electronic configuration. The unusual stability of the oxidation state was attributed to the accidental near-degeneracy of the two highest lying occupied molecular orbitals (π^* and δ^*) with three unpaired electrons and a high spin state (S = 3/2).[1,4] The unique electronic structure and physical properties are responsible for the growing expansion of the field of these and analogous compounds.[1,5] Potential applications comprise a wide variety of areas such as antitumor metallo drugs,[6,7] porous materials,[8,9] catalysts,[9,10] and supramolecular architectures[11] to develop new materials with mesogenic,[12] magnetic,[13] and electronic[14] properties.

The paddlewheel framework of the $[Ru_2(CH_3COO)_4Cl]$ dimer is shown in Figure 1. In the solid state, both axial positions are occupied by chloride ligands that axially bridge the dimetal units to give extended polymeric chains. In solution, the axial positions can be occupied by solvent molecules.[1] The tetrakis(acetato)chloridodiruthenium(II,III) complex and analogues such as the butanoato derivative are important synthetic precursors since the substitution of the bridging carboxylates offers a versatile route to novel $[Ru_2]^{5+}$ complexes with different carboxylates or other types of bridging ligands. In addition, the axial chlorido ligands can be removed upon

Received: January 22, 2012
Published: June 1, 2012

dx.doi.org/10.1021/ic300168t | Inorg. Chem. 2012, 51, 6615−6625

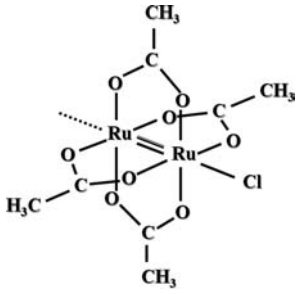

Figure 1. Structure of the dimeric unit $[Ru_2(CH_3COO)_4Cl]$.

reaction with silver salts, leaving both of the axial positions of the dimetal unit available for coordination by solvent molecules, and these can further be substituted by neutral *O*-, *N*- or *S*-donor ligands such as dimethylsulfoxide,[15] *N*-heterocyclic bases,[16] urea,[17] and tetrahydrothiophene,[18] to form new axially substituted compounds.[1] The majority of the investigations, however, report structural studies, whereas information on reactivity and kinetics has not received much attention for this class of compounds.[1]

Our group is interested in the chemical and biological properties of diruthenium(II,III) complexes. We have succeeded in using the precursor $[Ru_2(CH_3COO)_4Cl]$ to prepare a novel class of metallo drugs of the form $[Ru_2(dNSAID)_4Cl]$, *d*NSAID = deprotonated nonsteroidal anti-inflammatory drug, which shows interesting anti-inflammatory[19] and antitumor properties.[7,20,21] The Ru_2(II,III)-*d*NSAIDs and also a Ru_2(II,III)-(γ-linoleniccarboxylato)[7,22] drug were found to inhibit proliferation of the rat glioma C6 cell that is a model for the malignant brain tumor glioblastoma multiforme. Investigation of cellular response and signaling pathways showed that their antitumor activity might involve the mechanism of apoptosis.[20,22]

In general, in a physiological environment, metal complexes can undergo a variety of reactions and ligand substitution is one of the most important. The role of these reactions on the biological activity depends on the thermodynamic and kinetic behavior of the metal complex.[23] The exchange of chlorido ligands for water molecules (aquation) was found to be an important step for the biological activity of the ruthenium drug candidate NAMI-A, (Him) *trans*-$[RuCl_4(dmso)(im)]$, im = imidazole.[24] Hydrolysis involving water/chloride substitution is also a key reaction for the action of the antitumor cisplatin in clinical use.[25] The interactions of metal−metal bonded antitumor active compounds, in particular of dirhodium complexes, with DNA fragments and DNA have been investigated.[26] Antitumor metal-based drugs can interact with several other potential biomolecule targets[27,28] such as human serum albumin (HSA) and transferrin which might also play an important role in the biological activity of ruthenium drugs. The majority (80−90%) of ruthenium species in the bloodstream have been found to bind HSA.[27,29] This protein accumulates in tumor tissues and has also been investigated as the carrier conjugate of anticancer ruthenium drugs.[30] Transferrin was found to play an important role in the mode of action of the ruthenium drug candidate KP1019, (Hind) *trans*-$[RuCl_4(ind)_2]$, ind = indazole.[28,31] Preliminary studies on the interactions of Ru_2-*d*NSAIDs with plasma proteins, performed in our laboratories, have shown that Ru_2-ibuprofen interacts with HSA.[21]

Here we report studies on the thermodynamics of axial ligand substitution reactions and on the kinetic reactivity toward amino acids for the tetrakis(acetato)chlorido-diruthenium(II,III) complex. Since this synthetic precursor is more soluble than the corresponding Ru_2-*d*NSAIDs derivatives, the $[Ru_2(CH_3COO)_4]^+$ framework has been selected as a starting prototype model for the $[Ru_2(dNSAID)_4]^+$ paddle-wheel analogues.

EXPERIMENTAL SECTION

Materials. All chemicals used were of analytical-reagent grade and of the highest purity commercially available. $RuCl_3{\cdot}nH_2O$, LiCl, $AgPF_6$, and the amino acids glycine (gly), cysteine (cys), tryptophan (trp), and histidine (his) were purchased from Aldrich. Acetic anhydride and glacial acetic acid were purchased from Merck. For all preparations of aqueous solutions, deionized water was used.

Synthesis of $[Ru_2(CH_3COO)_4Cl]$. The compound was prepared by modification of a reported procedure.[32] $RuCl_3{\cdot}nH_2O$ (5.20 g) was dissolved in a previously distilled mixture of acetic anhydride (12 mL) and glacial acetic acid (45 mL) to which anhydrous lithium chloride (0.53 g) was added. The solution was stirred under an oxygen atmosphere at ∼60 °C for 24 h. The brown solid was separated by filtration, washed with acetone, and dried in a vacuum desiccator over phosphorus pentoxide. Yield, 80%. Anal. calc. for $C_8ClH_{12}O_8Ru_2$: C, 20.2; H, 2.5%. Found: C, 20.0; H, 2.4%. Magnetic measurements (μ_{eff}, 3.9 μ_B) and FTIR data (main bands: $\nu_{s(COO)}$, 1402 cm^{-1}; $\nu_{a(COO)}$, 1446 cm^{-1}) were in agreement with data reported before.[1,5]

Solutions of Diaqua-Ru_2 Species. The $[Ru_2(CH_3COO)_4Cl]$ compound was dissolved in water, the chloride ions were stoichiometrically precipitated with $AgPF_6$, and the solid AgCl was filtered off. The filtrate containing $[Ru_2(CH_3COO)_4(H_2O)_2]^+$ species showed a pH of 5.0.

Instrumentation and Measurements. *Characterization of $[Ru_2(CH_3COO)_4Cl]$.* Elemental analyses were performed on a Perkin-Elmer CHN 2004 Elemental Analyzer, Institute of Chemistry, University of São Paulo. A Fourier-Transform Infrared (FTIR) spectrum (4000−400 cm^{-1}) of solid dispersed in KBr was registered on a Bomen MB-102 spectrophotometer coupled to a diffuse reflectance accessory (Pike Technologies Inc.). Molar magnetic susceptibility was measured on powdered samples at room temperature by the Faraday method.[20]

Thermodynamic Studies on the Axial Substitution Reaction for the Diaqua-Ru_2 Species: Determination of Equilibrium Constants. Spectra were recorded on a Shimadzu UV 250 spectrophotometer at ambient pressure and 25 °C. Aqueous solutions of NaCl (from 0.10 to 0.40 mol L^{-1}, pH adjusted to about 5) were mixed with solutions of the diaqua-Ru_2 species (1 mmol L^{-1}, pH 5.0) in a tandem cuvette, and the equilibrium constant K_1 was determined by monitoring the absorbance changes at 440 nm. A similar procedure was followed for the equilibrium constant K_2 for 0.1 to 2.0 mol L^{-1} NaCl by monitoring absorbance changes at 455 nm.

Determination of Thermodynamic Standard Reaction Parameters. The equilibrium reactions were monitored as function of temperature to calculate the standard reaction enthalpy ($\Delta H°$) and entropy ($\Delta S°$), and also as a function of pressure to calculate the standard reaction volume ($\Delta V°$).[33] Absorbance changes in the temperature range 10−49 °C were monitored for two separate solutions of the diaqua-Ru_2species (1.0 mmol L^{-1}) to which an excess of chloride, 100 and 500 mmol L^{-1}, was added. Spectra were recorded on a Shimadzu Model UV-2101 PC UV−vis spectrophotometer equipped with a thermostatted cell holder. Absorbance changes in the pressure range 5−150 MPa at 28 °C were monitored for two separate solutions of the diaqua-Ru_2species (0.5 mmol L^{-1}) to which an excess of chloride, 50 and 250 mmol L^{-1}, was added. Spectra were recorded on the Shimadzu Model UV-2101 PC UV−vis spectrophotometer equipped with a custom-built high pressure cell and the use of a quartz pill-box cuvette.[34] Calculation of equilibrium constants at different temperatures and pressures were based on changes in absorbance by considering the following values of the molar extinction coefficients, ε

dx.doi.org/10.1021/ic300168t | *Inorg. Chem.* 2012, 51, 6615−6625

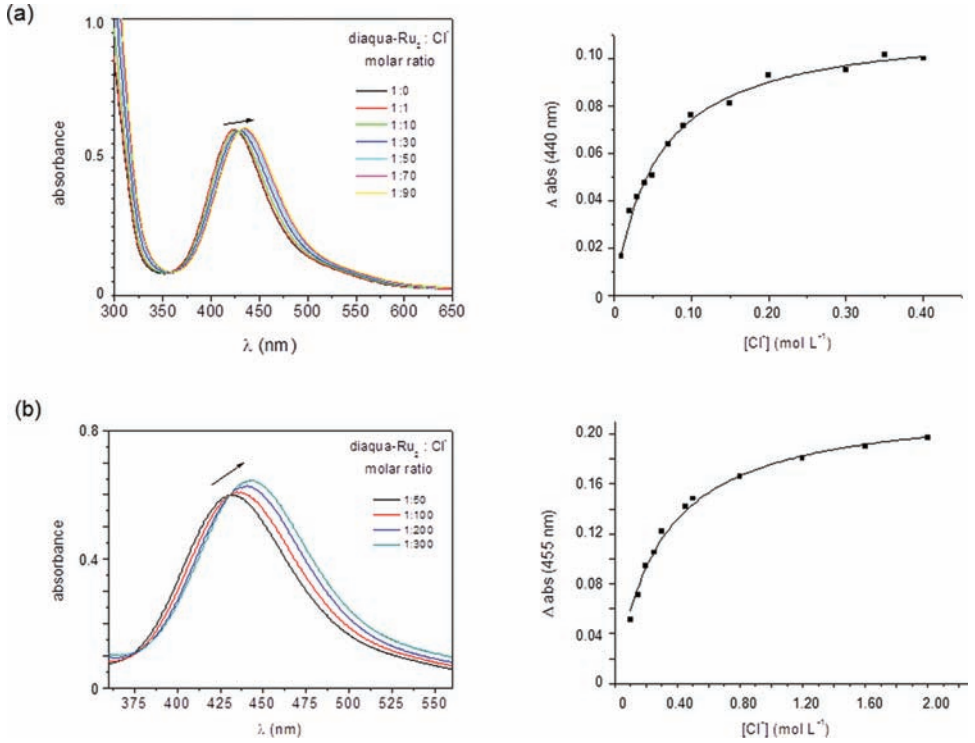

Figure 2. Spectra and corresponding plots of absorbance change versus chloride concentration for the subsequent addition of excess chloride relative to the starting diaqua-Ru_2 solution (1.0×10^{-3} mol L^{-1}, pH 5.0): (a) 0–90-fold excess of chloride; (b) 50–300-fold molar excess of chloride.

(mol^{-1} L cm^{-1}), for the diaqua-Ru_2, aqua(chlorido)-Ru_2, and dichlorido-Ru_2 species, respectively: 755, 563, 395 (at 423 nm); 748, 635, 485 (at 429 nm); 717, 680, 549 (at 434 nm); 659, 711, 608 (at 440 nm); 609, 720, 646 (at 445 nm); and 550, 710, 665 (at 450 nm).

Kinetic Studies on Reactions with Amino Acids. Kinetic measurements on slow reactions were performed on Shimadzu UV-2101 PC (for gly and his) or Shimadzu UV-1650 PC (for trp) spectrophotometers both equipped with thermostatted cell holders. Solutions of $[Ru_2(CH_3COO)_4(H_2O)_2]^+$ and amino acids (1 mL of each) were mixed in a tandem cuvette and spectra were recorded. Kinetic measurements on fast reactions (for cys) were performed by injecting both solutions directly in an Applied Photophysics SX 18MV stopped-flow instrument. The temperature of the instruments was controlled throughout all kinetic experiments to an accuracy of 0.1 °C. Acetate buffer (0.02 mol L^{-1}) was used to maintain pH 5.0. The conditions for the reactions with the amino acids (*aa*) were as follows. *Glycine*: (a) spectra were monitored for the time ranges 0 −1 h and 1−10 h, 7.0×10^{-4} mol L^{-1} Ru_2 complex, and 3.5×10^{-2} mol L^{-1} *aa*, pH 5.0, 25 °C; (b) kinetic traces were followed at 545 nm, 4.0×10^{-4} mol L^{-1} Ru_2, and $(8–32) \times 10^{-3}$ mol L^{-1} *aa*, pH 5.0, 25 °C. *Cysteine*: (a) spectra were monitored for the time ranges 0−1, 1−30, and 40−500 s, 2.0×10^{-4} mol L^{-1} Ru_2, and 2.0×10^{-3} mol L^{-1} *aa*, pH 5.0, 25 °C; (b) kinetic traces were followed at 354 nm, 1.0×10^{-4} mol L^{-1} Ru_2, and $(1.0–4.5) \times 10^{-3}$ mol L^{-1} *aa*, pH 5.0, 10 °C; (c) kinetic traces were also followed at 460 nm, 1.0×10^{-4} mol L^{-1} Ru_2, and $(2.0–20.0) \times 10^{-3}$ mol L^{-1} *aa*, pH 5.0, 25 °C. *Tryptophan:* (a) spectra were monitored for the time range 0−300 s, 2.0×10^{-4} mol L^{-1} Ru_2, and 8.0×10^{-3} mol L^{-1} *aa*, pH 5.0, 25 °C; (b) kinetic traces were followed at 545 nm, 2.0×10^{-4} mol L^{-1} Ru_2, and $(2.0–16.0) \times 10^{-3}$ mol L^{-1} *aa*, pH 5.0, 25 °C. *Histidine*: (a) spectra were monitored for the time range 0−300 s, 2.0×10^{-4} mol L^{-1} Ru_2, and 8.0×10^{-3} mol L^{-1} *aa*, pH 5.0, 25 °C; (b) spectra were also followed for the time ranges 0−10 and 0−1200 s, 2.0×10^{-4} mol L^{-1} Ru_2, and 20.0×10^{-3} mol L^{-1} *aa*, pH 4.3, 25 °C; (c) kinetic traces were followed at 545 nm, 2.0×10^{-4} mol L^{-1} Ru_2, and $(5.0–20.0) \times 10^{-3}$ mol L^{-1} *aa*, pH 5.0, 25 °C. In all experiments, the amino acids were at least in a 10-fold molar excess with respect to the Ru_2 complex. The reported pseudofirst-order rate constants were calculated based on the average values of at least three independent kinetic measurements. The observed rate constants (k_{obs}) were calculated based on kinetic traces which were fitted to single or double exponential functions obtained by using OriginPro8 (Originlab Corporation) software (examples of kinetic traces and equations are shown in the Supporting Information).

RESULTS AND DISCUSSION

Electronic spectra of $[Ru_2(R_2COO)_4Cl]$ paddlewheel complexes show bands in the UV (250–350 nm), visible (420–480 nm), and NIR (900–1200 nm) regions.[1,4,35,36] Two intense UV bands at ~220–350 nm are proposed to have a strong contribution of a LMCT $\sigma \rightarrow \sigma^*$ electronic transition supported by a significant red shift on exchanging axial chloride for other X halide ligands such as bromide and iodide in $[Ru_2(RCOO)_4X_2]^-$ species.[36] The visible band is assigned to the $\pi(Ru–O) \rightarrow \pi^*(Ru_2)$ electronic transition, while the low intensity NIR band is attributed to the $\delta(Ru_2) \rightarrow \delta^*(Ru_2)$ transition. The λ_{max} of the visible transition is fairly dependent on the nature of the coordinating axial ligand. The transition is detected at $\lambda_{max} \sim 470$ nm for solid polymeric species and approximately the same value is found for the anionic dichlorido-Ru_2, $[Ru_2(RCOO)_4Cl_2]^-$, chromophore in solution containing excess chloride ions. In noncoordinating solvents such as CH_2Cl_2, the band shifts to higher energy (~450 nm) due to the presence of the solvent-chlorido-Ru_2, $[Ru_2(RCOO)_4Cl(Sol)]$, main chromophore. In coordinating and polar solvents such as MeOH, the shift (~430 nm) is more significant due to the predominance of the cationic disolvent-Ru_2, $[Ru_2(RCOO)_4(Solv)_2]^+$, main chromophore. TDDFT (Time Dependent Density Functional Theory) and TDDFT-PCM (Polarized Continuum Model) calculations for $[Ru_2(RCOO)_4Cl_2]^-$ in vacuum and in acetonitrile, respectively,[37] agree with previous assignments[35] that the band at ~470 nm shifts to higher energy in solution. Therefore,

dx.doi.org/10.1021/ic300168t | *Inorg. Chem.* 2012, 51, 6615–6625

equilibration reactions of axial substitution play an important role in the chemical behavior of these complexes.

Thermodynamic Studies on the Axial-Substitution Reaction for Diaqua-Ru_2 Species. The first part of the thermodynamic studies was the reinvestigation of the two successive equilibration reactions 1 and 2 with the determination of the equilibrium constants (K_{eq}) for the first (K_1) and second (K_2) axial substitutions of $[Ru_2(CH_3COO)_4(H_2O)_2]^+$ in the presence of chloride ions. Spectrophotometric titrations by addition of increasing concentrations of chloride to diaqua-Ru_2 solutions were performed to follow the changes in absorbance (Δ_{abs}) of the visible band assigned to the π(Ru−O) → π^*(Ru_2) transition. In the first experiment, the addition of chloride from a Ru_2:Cl^- molar ratio of 1:0 to 1:90 was accompanied by a band shift from 425 to 435 nm that indicated the axial substitution of one water molecule by the chloride (Figure 2). The presence of two isosbestic points (at 359 and 428 nm) gave evidence for the first equilibrium between the cationic diaqua-Ru_2 and the neutral aqua(chlorido)-Ru_2 species represented by eq 1. In the second experiment, a starting solution containing predominantly the aqua(chlorido)-Ru_2 species was prepared by addition of a 50-fold molar excess of chloride over diaqua-Ru_2 and spectral changes were followed from a Ru_2:Cl^- ratio of 1:50 by subsequent addition of chloride up to a 300-fold molar excess of chloride. The visible band shifted from 435 to 445 nm, suggesting the axial substitution of the second water molecule to give the anionic dichlorido-Ru_2 complex. The existence of two novel isosbestic points (at 375 and 431 nm) gave evidence for the second equilibrium represented by eq 2.

$$[Ru_2(CH_3COO)_4(H_2O)_2]^+ + Cl^- \overset{K_1}{\rightleftharpoons} [Ru_2(CH_3COO)_4Cl(H_2O)] + H_2O \quad (1)$$

$$[Ru_2(CH_3COO)_4Cl(H_2O)] + Cl^- \overset{K_2}{\rightleftharpoons} [Ru_2(CH_3COO)_4Cl_2]^- + H_2O \quad (2)$$

The values of the equilibrium constants K_1 and K_2 were calculated according to eq 3, where A_o and A_∞ represent the initial and final absorbance, respectively, and A_x is the absorbance value at any chloride concentration.

$$A_x = A_o + \{(A_\infty - A_o)K_{eq}[Cl^-]\}/\{1 + K_{eq}[Cl^-]\} \quad (3)$$

Linear plots of the change in absorbance ($\Delta_{abs} = A_x - A_o$) as function of chloride concentration were obtained and allowed the calculation of the equilibrium constants K_1 (at 440 nm) and K_2 (at 455 nm). The calculated values (see Table 1) are 18 ± 1 mol^{-1} L (K_1) and 3.5 ± 0.2 mol^{-1} L (K_2), which are in close agreement with those reported before, viz. 15 ± 1 mol^{-1} L (K_1) and 3.7 ± 0.3 mol^{-1} L (K_2) that were calculated from absorbance measurements at 290 nm and 25 °C.[37] The equilibrium constant for reaction 1 is about 5-fold higher than that for reaction 2 and indicates that substitution of the first water molecule by chloride to form the neutral aqua(chlorido)-Ru_2 species is more favorable than the second substitution process.

The effect of the temperature, from 10 to 49 °C, on reactions 1 and 2 was followed by spectral monitoring (Figure 3) to calculate the standard reaction parameters $\Delta H°$ and $\Delta S°$. To study equilibrium 1, the starting solution was prepared to have a 100-fold molar excess of chloride over the diaqua-Ru_2 complex to guarantee the predominance of the aqua(chlorido)-Ru_2 species. The intensity of the band at 435 nm decreased as the temperature was increased, suggesting that at higher temperatures equilibrium 1 shifts in the backward direction to transform the aqua(chlorido)-Ru_2 species back into the diaqua-Ru_2 species. For equilibrium 2, the starting solution had a 500-fold molar excess of chloride over the diaqua-Ru_2species to guarantee the predominance of the dichlorido-Ru_2 species. The intensity of the band at 445 nm also decreased on increasing temperature, suggesting that at higher temperatures equilibrium 2 shifts in the reverse direction to transform the dichlorido-Ru_2species back into the aqua(chlorido)-Ru_2 species. Linear plots of $R \ln K_{eq}$ versus $1/T$ (Figures S1a and S1b, Supporting Information) enabled the calculation of $\Delta H°$ and $\Delta S°$ (see Table 1) from the slope and intercept, respectively, according to eq 4.

$$R \ln K_{eq} = (-\Delta H°/T) + \Delta S° \quad (4)$$

The pressure dependence of the equilibrium constants was studied at pressures from 5 up to 150 MPa at 28 °C. To study equilibrium 1, the starting solution had a 100-fold molar excess of chloride over the diaqua-Ru_2 species to guarantee the predominance of the aqua(chlorido)-Ru_2 species. The intensity of the band at 430 nm slightly increased with increasing pressure. For equilibrium 2, the starting solution had a 500-fold molar excess of chloride over the diaqua-Ru_2 species to guarantee the predominance of the dichlorido-Ru_2 species. The intensity of the band at 440 nm also showed a slight increase with increasing pressure. The increase in the intensity of the band at 430 nm on increasing pressure suggests that at higher pressures equilibrium 1 is shifted in the forward direction to transform the diaqua-Ru_2 species into aqua(chlorido)-Ru_2 species. The intensity of the band at 440 nm also increased on increasing pressure, suggesting that at higher pressures equilibrium 2 also shifts in the forward direction, to transform the aqua(chlorido)-Ru_2 species into the dichlorido-Ru_2 species. Linear plots of $R \ln K_{eq}$ as function of pressure (Figures S1c and S1d, Supporting Information) were obtained and showed that the values of both equilibrium constants 1 and 2 increase on increasing pressure. The plots enabled the calculation of $\Delta V°$ (see Table 1) from the slope according to eq 5.

$$\ln K_{(28°C)} = -(\Delta V° P/RT) + \text{constant} \quad (5)$$

On the basis of the standard reaction parameter values summarized for reactions 1 and 2 in Table 1, some conclusions can be proposed. Both equilibrium shift in the backward direction on increasing temperature, what is typical for exothermic reactions for which $\Delta H°$ has negative values.

Table 1. Equilibrium Constants (K) and Standard Reaction Parameters for Reactions 1 and 2 That Involve Axial Substitution of Water by Chloride in Diaqua-Ru_2

parameter	reaction 1	reaction 2
$K_{(25°C)}$ (mol^{-1} L)	18 ± 1	3.5 ± 0.2
$K_{(28°C)}$ (mol^{-1} L)	18 ± 1[a]	3.3 ± 0.4[a]
$K_{(28°C)}$ (mol^{-1} L)	18 ± 1[b]	3.2 ± 0.4[b]
$K_{(28°C)}$ (mol^{-1} L)	17[c]	3.2[c]
$\Delta H°$ (kJ mol^{-1})	−8.7 ± 0.5	−11.4 ± 0.5
$\Delta S°$ (J K^{-1} mol^{-1})	−5 ± 2	−28 ± 2
$\Delta V°_{(28°C)}$ (cm^3 mol^{-1})	−12 ± 2	−10.0 ± 0.8

[a]Calculated from the Gibbs−Helmholtz equation. [b]Based on the intercept from the pressure data. [c]Based on the lowest pressure data at 0.1 MPa.

dx.doi.org/10.1021/ic300168t | Inorg. Chem. 2012, 51, 6615−6625

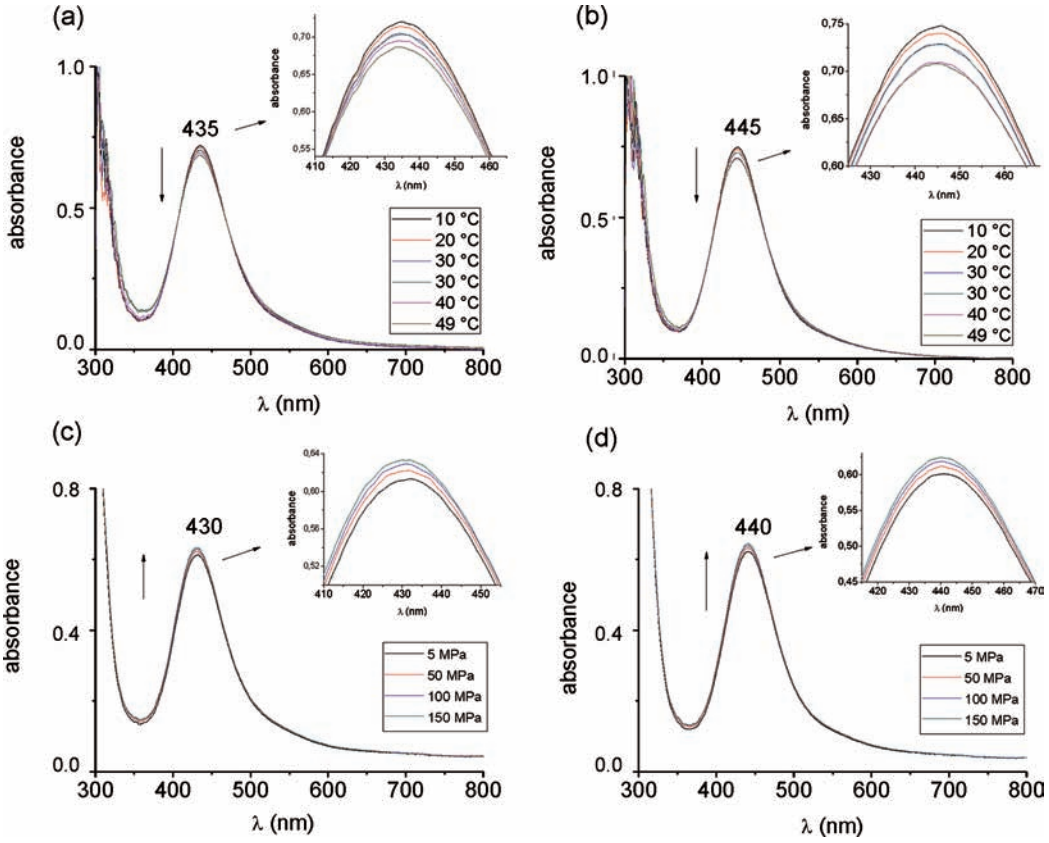

Figure 3. Spectral changes for temperature dependence (10−49 °C) of diaqua-Ru_2 solution (1.0×10^{-3} mol L^{-1}) with: (a) 100-fold molar excess of chloride; (b) 500-fold molar excess of chloride. Spectral changes for pressure dependence (5−150 MPa) of diaqua-Ru_2 solution (5.0×10^{-4} mol L^{-1}) with: (c) 100-fold molar excess of chloride; (d) 500-fold molar excess of chloride.

Therefore, both of the subsequent axial substitution reactions of water for chloride are enthalpy driven. Reaction 2 is slightly more enthalpy-driven than reaction 1, which is consistent with the formation of the stronger ruthenium-axial bonds that would be expected for coordination of ruthenium to chloride in comparison with coordination to water. $\Delta S°$ has negative values indicating that both reactions 1 and 2 are not entropy driven. On increasing pressure both reactions 1 and 2 shift in the forward direction. This can be explained by a decrease in the partial molar volume of the products on the axial substitution of water by chloride. The more negative value of $\Delta S°$ found for reaction 2 can be ascribed to the increase in electrostriction of the solvent shell during the formation of the dichlorido complex.

The values for K_1 and K_2 calculated from the Gibbs−Helmholtz equation for 28 °C were 18 and 3.3, respectively. On the basis of the intercept from the pressure data, K_1 and K_2 values were found to be 18 and 3.2, respectively, and based on the lowest pressure data (0.1 MPa), the K_1 and K_2 values are 17 and 3.2, respectively (see Table 1). It follows that the pressure dependent data are in very close agreement with the temperature dependent data extrapolated to 28 °C.

Kinetic Studies on Reactions with Amino Acids. Prior to the kinetic studies performed for reactions with a series of amino acids, we also tried to study the reaction of diaqua-Ru_2 with chloride, i.e. reactions 1 and 2. However, the reaction is too fast for stopped-flow measurements even at lower temperatures, and occurs within the mixing time of the instrument. This is due to the high concentration of chloride that is required because of the unfavorable equilibrium position (and small absorbance changes) associated with this reaction. The reaction would in principle be slower at lower chloride concentrations, but then the absorbance changes are too small to measure. Similar observations were reported in the literature.[37] The reactions with the amino acids were in general found to be much slower and could be studied at lower concentrations, such that there were no further complications.

Reaction with Glycine. The kinetic results for the reaction of diaqua-Ru_2 with glycine are shown in Figure 4. The solution of the diaqua-Ru_2 species was mixed with a 50-fold molar excess of glycine and spectral changes were monitored as a function of time. During the first hour of the reaction, the band at 425 nm shifted to lower energy and decreased in intensity, while a new band appeared at 540 nm. The deconvolution of the spectrum (Figure S2, Supporting Information) recorded at the end of 1 h of the reaction suggested that the band at 423 nm was still present while two new visible bands, at 465 and 540 nm, could be assigned to a new chromophore. The observed kinetic traces fitted to a single exponential function, and the plot of the observed rate constant (k_{obs}) (see Table S1, Supporting Information) as function of the glycine concentration fitted to eq 6 to give the rate constants $k_1 = (1.95 \pm 0.09) \times 10^{-2}$ mol^{-1} L s^{-1} and $k_{-1} = (1.7 \pm 0.2) \times 10^{-4}$ s^{-1} (see Table 2).

$$k_{obs} = k_1[gly] + k_{-1} \quad (6)$$

The linear increase in both k_{obs} and the observed absorbance change at 545 nm with increasing glycine concentration, which can also be seen from the observed kinetic traces on increasing the glycine concentration, indicates the occurrence of a reversible reaction. The reversible reaction is suggested to be

dx.doi.org/10.1021/ic300168t | Inorg. Chem. 2012, 51, 6615−6625

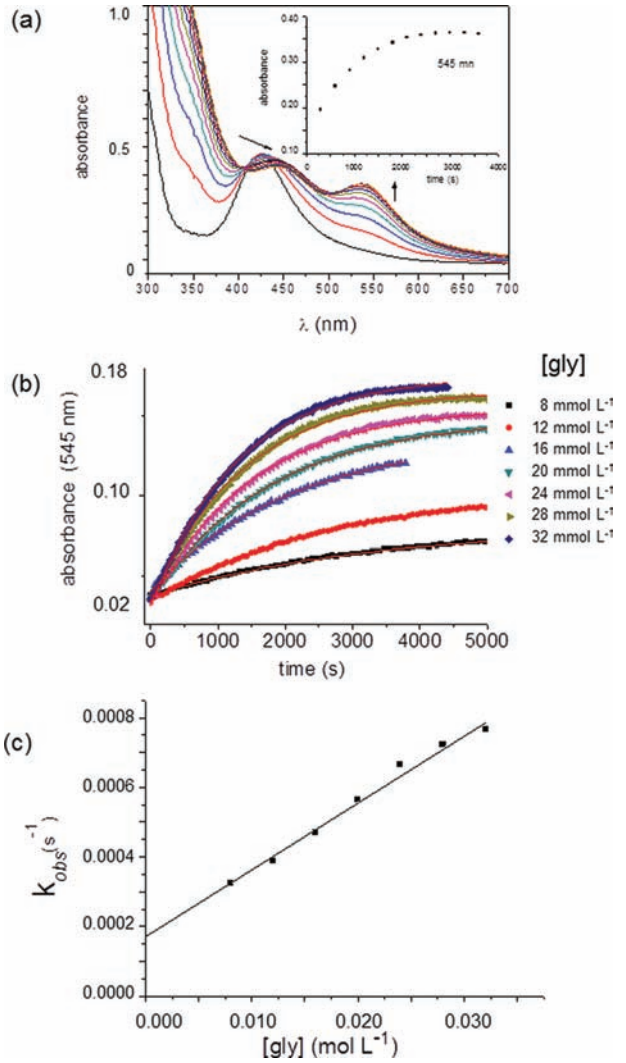

Figure 4. Kinetic studies for the reaction with glycine. (a) Spectra recorded after the addition of a 50-fold excess of glycine (3.5×10^{-2} mol L^{-1}) to diaqua-Ru_2 (7.0×10^{-4} mol L^{-1}) solution over the time range 0−1 h, 25 °C, pH 5.0. (inset) Kinetic trace at 545 nm. (b) Kinetic traces recorded for diaqua-Ru_2 (4.0×10^{-4} mol L^{-1}) solution with different concentrations of glycine at 545 nm, 25 °C, pH 5.0. (c) Glycine concentration dependence of k_{obs} for diaqua-Ru_2 (4.0×10^{-4} mol L^{-1}) solution with different concentrations of glycine, 545 nm, 25 °C, pH 5.0.

related to the axial substitution of water in the diaqua-Ru_2 species to form the aqua(gly)-Ru_2 species as the main product. The overall equilibrium constant, $K_1 = k_1/k_{-1}$, was calculated to be $(1.1 \pm 0.2) \times 10^2$ mol^{-1} L.

The subsequent spectral changes observed during 1−10 h of the reaction (Figure S3, Supporting Information) are suggested to present a second step that involves the slow decomposition of the aqua(gly)-Ru_2 species. Deconvolution of the final spectrum (Figure S4, Supporting Information) indicated an intensity decrease of the bands at 465 and 540 nm and showed that the band at 423 nm is still present even after 10 h reaction time, which suggests that a considerable amount of the diaqua-Ru_2 species still remained in solution and did not react with the amino acid. This is in agreement with the reversibility of the first reaction step as discussed above. The overall reaction scheme is summarized in reactions 7 and 8.

Table 2. Kinetic Data for the Reaction of Diaqua-Ru_2 with Different Amino Acids at 25 °C[a]

amino acid	rate constant (k)	equilibrium constant
glycine	$k_1 = (1.95 \pm 0.09) \times 10^{-2}$ L mol^{-1} s^{-1}	$K_1 = (1.1 \pm 0.2) \times 10^2$ L mol^{-1}
	$k_{-1} = (1.7 \pm 0.2) \times 10^{-4}$ s^{-1}	
cysteine	$k_1 = (6.5 \pm 0.1) \times 10^3$ L mol^{-1} s^{-1}	$K_1 = (1.3 \pm 0.5) \times 10^4$ L mol^{-1}
	$k_{-1} = 0.5 \pm 0.2$ s^{-1}	
	$K_1k_2 = (4.6 \pm 0.5) \times 10^2$ L^2 mol^{-2} s^{-1}	$K_1K_2 = (5.1 \pm 0.9) \times 10^3$ L^2 mol^{-2}
	$k_{-2} = (8.92 \pm 0.01) \times 10^{-2}$ s^{-1}	
tryptophan	$k_1 = (4.9 \pm 0.2) \times 10^{-2}$ L mol^{-1} s^{-1}	$K_1 = (1.4 \pm 0.1) \times 10^2$ L mol^{-1}
	$k_{-1} = (3.4 \pm 0.2) \times 10^{-4}$ s^{-1}	
histidine	$K_1k_2 = (2.5 \pm 0.1) \times 10^3$ L^2 mol^{-2} s^{-1}	$K_1K_2 = (8.7 \pm 0.4) \times 10^6$ L^2 mol^{-2}
	$k_{-2} = (2.86 \pm 0.01) \times 10^{-4}$ s^{-1}	
	$k_3 = 4.7 \pm 0.1$ L mol^{-1} s^{-1}	

[a]Except for the first reaction step with cysteine at 10 °C.

$$[Ru_2(CH_3COO)_4(H_2O)_2]^+ + {}^+H_3NCH_2COO^- \underset{k_{-1}}{\overset{k_1}{\rightleftharpoons}} [Ru_2(CH_3COO)_4(H_2O)(H_2NCH_2COO)] + H_3O^+ \quad (7)$$

$$[Ru_2(CH_3COO)_4(H_2O)(H_2NCH_2COO)] \xrightarrow{\text{slow}} \text{decomposition products} \quad (8)$$

Glycine has two available sites to coordinate to metal ions, viz. the carboxylate (COO) and the amine (NH_2) groups. Since the pK_a values are 2.34 and 9.58 for the carboxylic acid and the amino moieties,[38] respectively, the carboxylic acid group is mainly deprotonated at pH 5, whereas the amino group is mainly protonated, and glycine is mostly present in the neutral $^+H_3N-CH_2-COO^-$ form. Therefore, the reversible reaction 7 involves coordination of glycine to the ruthenium center via the carboxylate group. However, the appearance of new visible bands led us to also consider coordination of glycine through the nitrogen atom. This possibility cannot be ruled out and a possible explanation might be an intramolecular linkage isomerization from CO**O**− to −**N**H_2. Once glycine coordinates to ruthenium through the oxygen atom of the carboxylate group, the pK_a value of the NH_3^+ group is expected to decrease, leaving the nitrogen atom deprotonated and available for coordination to the metal center. To investigate this possibility, nonbuffered (initial pH 5.0) solutions of the complex and glycine were mixed, and the pH was monitored and showed a steady decrease as a function of time. This result suggests that the studied reaction lowers the pH of the solution, most probably due to the release of protons during the coordination of glycine as shown in reaction 7. Decomposition products from the slow subsequent reaction 8 could include monomeric species resulting from disruption of the paddlewheel framework.

Reaction with Cysteine. The kinetic results for the reaction of diaqua-Ru_2 with cysteine are shown in Figures 5 and 6. The starting solution of diaqua-Ru_2 was mixed with a 10-fold molar excess of cysteine and spectral changes were monitored as a function of time. The spectral changes recorded within the first second of the reaction showed two new absorption bands at ~350 and 470 nm (Figure 5). Subsequent spectral changes

dx.doi.org/10.1021/ic300168t | Inorg. Chem. 2012, 51, 6615−6625

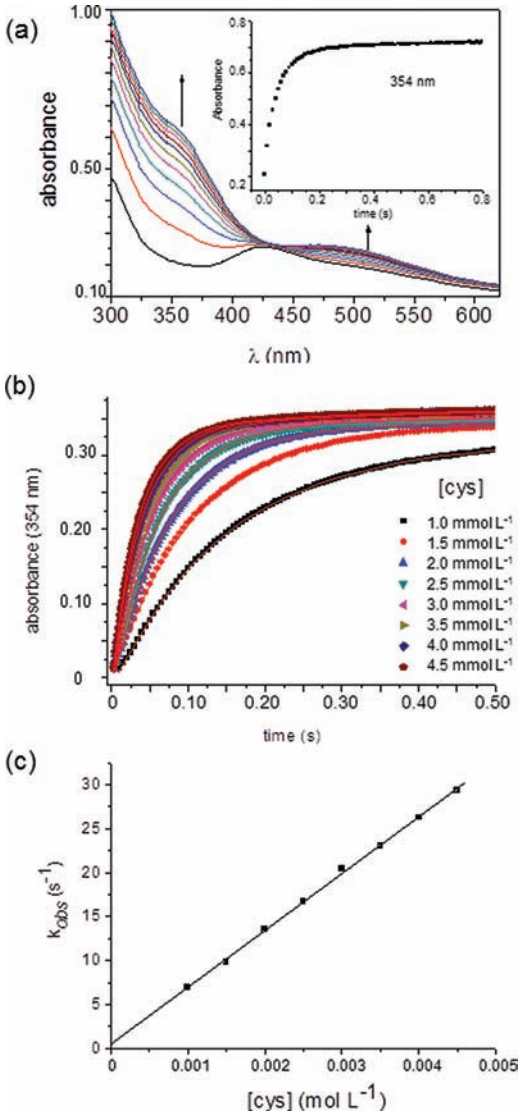

Figure 5. Kinetic studies for the reaction with cysteine. (a) Spectra recorded after 10-fold molar excess addition of cysteine (2.0×10^{-3} mol L^{-1}) to diaqua-Ru_2 (2.0×10^{-4} mol L^{-1}) solution during the time range 0−1 s, 25 °C, pH 5.0. (inset) Kinetic trace at 354 nm. (b) Kinetic traces recorded for diaqua-Ru_2 (1.0×10^{-4} mol L^{-1}) solution with different concentrations of cysteine at 354 nm, 10 °C, pH 5.0 (first step). (c) Concentration dependence of k_{obs} (for diaqua-Ru_2 (1.0×10^{-4} mol L^{-1}) solution with different concentrations of cysteine, 354 nm, 10 °C, pH 5.0.

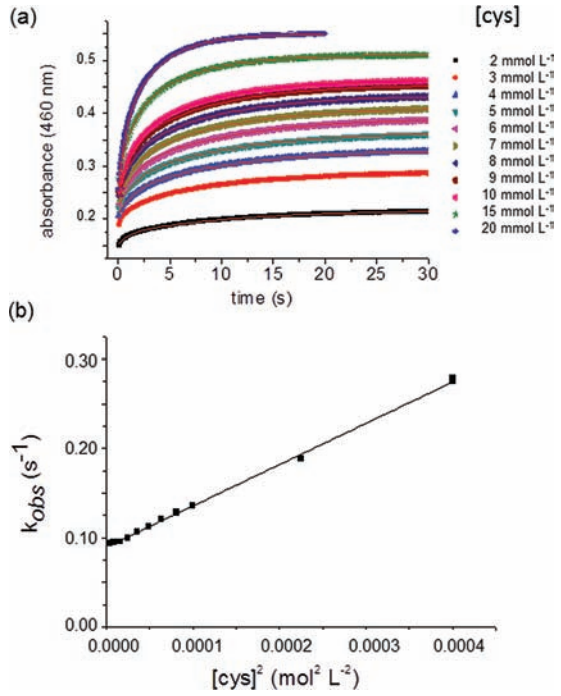

Figure 6. Kinetic studies for the reaction with cysteine. (a) Kinetic traces recorded for diaqua-Ru_2 (1.0×10^{-4} mol L^{-1}) solution with different concentrations of cysteine at 460 nm, 25 °C, pH 5.0 (second step). (b) Concentration dependence of k_{obs} for diaqua-Ru_2 (1.0×10^{-4} mol L^{-1}) solution with different concentrations of cysteine, 460 nm, 25 °C, pH 5.0.

(Figure S5a, Supporting Information) during the time range 1−30 s showed a slight intensity increase of the band at ∼350 nm and a shift of the band at 480 nm to smaller wavelengths (deconvolution of the final spectrum for the first step is shown in Figure S6, Supporting Information). Following this, during the time range 40−500 s, the intensity of the band at 480 nm decreased and an isosbestic point appeared at 450 nm (Figure S5b, Supporting Information). The kinetics of the first and second reactions was investigated by stopped-flow technique under pseudofirst-order conditions. The first faster reaction could be attributed to axial substitution of one water molecule in the diaqua-Ru_2 species by cysteine, whereas the second reaction could be assigned to the displacement of the second water molecule. The second reaction is significantly slower than the first one, even at the highest temperature. The kinetic traces were followed as a function of cysteine concentration (for observed rate constants (k_{obs}) values; see Table S2, Supporting Information) at 354 nm and fitted to a single exponential function. The overall absorbance change and the kinetic behavior suggest an almost irreversible reaction for which the rate law is given by eq 9. From the plot in Figure 5c, it follows that $k_1 = (6.5 \pm 0.1) \times 10^3$ L mol^{-1} s^{-1} and $k_{-1} = 0.5 \pm 0.2$ s^{-1} at 10 °C (see Table 2), with $K_1 = k_1/k_{-1} = (1.3 \pm 0.5) \times 10^4$ L mol^{-1}, which clearly demonstrates the very efficient formation of the (aqua)cys-Ru_2 complex.

$$k_{obs} = k_1[cys] + k_{-1} \quad (9)$$

The kinetic traces recorded for the time range 1−30 s (Figure 6a) clearly show the formation of an unfavorable equilibrium which is shifted to the dicysteine complex on increasing the cysteine concentration. The kinetic traces for this reaction followed at 460 nm were fitted to a double exponential function in order to correct for the interference of the first reaction step. Surprisingly, k_{obs} (see Table S3, Supporting Information) for the second reaction step showed a square dependence on the cysteine concentration, and the experimental data could be fitted with the rate law given in (10) as shown in Figure 6b. The plot of k_{obs} versus $[cys]^2$ resulted in $k_{on} = (4.6 \pm 0.5) \times 10^2$ L^2 mol^{-2} s^{-2} and $k_{off} = (8.92 \pm 0.01) \times 10^{-2}$ s^{-1} at 25 °C (Table 2).

$$k_{obs} = k_{on}[cys]^2 + k_{off} \quad (10)$$

The suggested reaction mechanism that can account for the observed kinetic data is outlined in reactions 11 and 12, where Hcys represents $HSCH_2CH(NH_3^+)COO^-$ is as follows:

dx.doi.org/10.1021/ic300168t | Inorg. Chem. 2012, 51, 6615−6625

$$[Ru_2(O_2CCH_3)_4(H_2O)_2]^+ + Hcys \underset{k_{-1}}{\overset{k_1}{\rightleftharpoons}} [Ru_2(O_2CCH_3)_4(H_2O)(cys)] + H_3O^+ \quad (11)$$

$$[Ru_2(O_2CCH_3)_4(H_2O)(cys)] + Hcys \underset{k_2}{\overset{k_2}{\rightleftharpoons}} [Ru_2(CH_3COO)_4(cys)_2]^- + H_3O^+ \quad (12)$$

The rate law for the second reaction step based on a steady state approximation for the intermediate 1:1 complex formed in reaction 11, is given in eq 13, which reduces to (14) under the conditions that $k_2[Hcys] \ll k_{-1}$.

$$k_{obs} = \frac{k_1k_2[Hcys]^2 + k_{-1}k_{-2}}{k_{-1} + k_2[Hcys]} \quad (13)$$

$$k_{obs} = K_1k_2[Hcys]^2 + k_{-2} \quad (14)$$

Equation 14 is in agreement with eq 10 where $k_{on} = K_1k_2 = (4.6 \pm 0.5) \times 10^2$ L^2 mol^{-2} s^{-2} and $k_{off} = k_{-2} = (8.92 \pm 0.01) \times 10^{-2}$ s^{-1}.

Cysteine has three possible binding sites for metal ions, viz. the carboxylate (COO), amine (NH_2), and thiol (SH) groups. The pK_a values of these groups are 1.91, 10.28, and 8.14,[38] respectively. Although the thiol group should be protonated at pH 5.0, the results suggest that it might be the main binding site of cysteine because of its strong donor character. Moreover, the final spectrum is different from that observed for the reaction with glycine. In a similar way to the reaction with glycine, the reaction with cysteine might involve an intramolecular linkage isomerization from CO**O**− to −**S**. The amino acid binding to ruthenium via the carboxylate anion can be followed by subsequent coordination of the sulfur to ruthenium due to a decrease in the pK_a value accompanied by deprotonation of the thiol group.

Reaction with Tryptophan. The kinetic results for the reaction of diaqua-Ru_2 with tryptophan are shown in Figure 7. The starting solution of diaqua-Ru_2 was mixed with a 50-fold molar excess of tryptophan. Spectral changes during the first hour of the reaction showed two new bands at 450 and 540 nm and a shoulder at 345 nm. Deconvolution (Figure S7, Supporting Information) of the final spectrum for this reaction showed the presence of three bands (465, 538, and 630 nm) that can be ascribed to the new chromophore. However, the band at 423 nm is still present and suggests that part of the original diaqua-Ru_2 species remained in solution. The kinetic traces recorded at 525 nm (Figure S8a, Supporting Information) nicely fitted a single exponential function and clearly showed evidence for an equilibration reaction as seen from the increase in the final absorbance as a function of the tryptophan concentration. The plot of the observed rate constant (k_{obs}) (see Table S4, Supporting Information) as function of tryptophan concentration fitted the rate law given in eq 15, and resulted in $k_1 = (4.9 \pm 0.2) \times 10^{-2}$ mol^{-1} L s^{-1} and $k_{-1} = (3.4 \pm 0.2) \times 10^{-4}$ s^{-1}, from which it follows that $K_1 = k_1/k_{-1} = (1.4 \pm 0.1) \times 10^2$ mol^{-1} L (see Table 2). These findings are in agreement with the reaction outlined in 16, where Htrp represents $^+H_3NC_2H_4(C_8H_5NH)COO^-$.

$$k_{obs} = k_1[trp] + k_{-1} \quad (15)$$

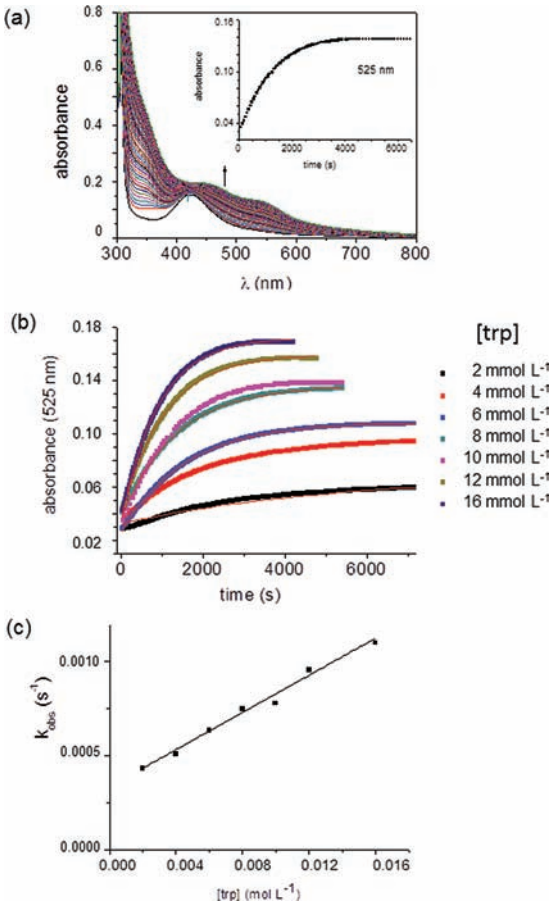

Figure 7. Kinetic studies for the reaction with tryptophan. (a) Spectra recorded after 40-fold molar excess of tryptophan (10×10^{-3} mol L^{-1}) added to diaqua-Ru_2 (2.0×10^{-4} mol L^{-1}) solution during the time range 0−1 h, 25 °C, pH 5.0. (inset) Kinetic curve at 525 nm. (b) Kinetic traces recorded for diaqua-Ru_2 (2.0×10^{-4} mol L^{-1}) solution with different concentrations of tryptophan, 525 nm, 25 °C, pH 5.0. (c) Concentration dependence of k_{obs} (for diaqua-Ru_2 (2.0×10^{-4} mol L^{-1}) solution with different concentrations of tryptophan, 525 nm, 25 °C, pH 5.0).

$$[Ru_2(O_2CCH_3)_4(H_2O)_2]^+ + Htrp \underset{k_{-1}}{\overset{k_1}{\rightleftharpoons}} [Ru_2(O_2CCH_3)_4(H_2O)(trp)] + H_3O^+ \quad (16)$$

Tryptophan also has three possible binding sites for metal ions: the carboxylate (COO), the amine (NH_2), and the indole (C_8H_5NH) groups. The pK_a values of these groups are 2.38 and 9.34,[38] for the carboxylic and the amino groups, respectively. The indole group of tryptophan seems to not have a significant effect on the reaction of the amino acid since the rate of the first step was only 2.5 times higher than that found for glycine. However, as for the reaction with glycine, an intramolecular linkage isomerization from CO**O**− to −**N**H_2 cannot be ruled out.

Reaction with Histidine. The kinetic results for the reaction of diaqua-Ru_2 with histidine are shown in Figure 8. The starting solution of diaqua-Ru_2 was mixed with a 40-fold molar excess of histidine. The observed spectral changes suggested the occurrence of two subsequent reactions. The first reaction is accompanied by an absorbance decrease of the band at 436 nm and the appearance of two new bands (~ 350 and 545 nm) and a shoulder (474 nm). The spectral changes during the

dx.doi.org/10.1021/ic300168t | Inorg. Chem. 2012, 51, 6615−6625

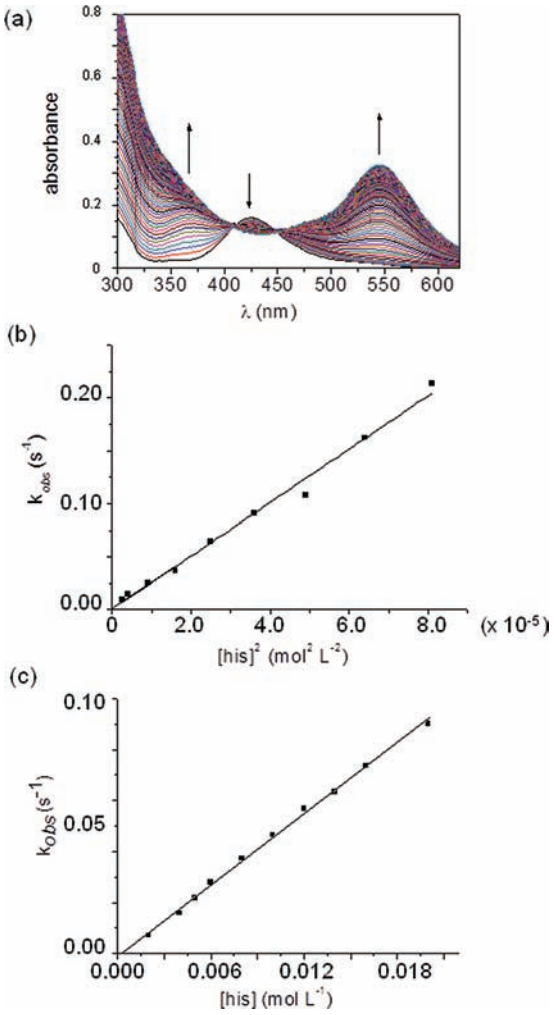

Figure 8. Kinetic studies for the reaction with histidine. (a) Spectra recorded after addition of 40-fold molar excess of histidine (8.0×10^{-3} mol L^{-1}) to diaqua-Ru_2 (2.0×10^{-4} mol L^{-1}) solution during the time range 0–300 s, 25 °C, pH 5.0. (b) Concentration dependence of k_{obs} (for diaqua-Ru_2 (2.0×10^{-4} mol L^{-1}) solution with different concentrations of histidine, 350 nm, 25 °C, pH 5.0) for the fast reaction. (c) Concentration dependence of k_{obs} (diaqua-Ru_2 (2.0×10^{-4} mol L^{-1}) solution with different concentrations of histidine, 545 nm, 25 °C, pH 5.0) for the slower reaction.

induction period (~10 s) showed two isosbestic points. Spectral changes for the second reaction showed a decrease in absorbance at 545 nm on increasing the histidine concentration. The kinetics of the reactions was studied at 350 nm for the first reaction (Figure S8b, Supporting Information) and at 545 nm for the second reaction. The kinetic traces were fitted to double exponential functions to be able to separate the two reaction steps (Figure S9, Supporting Information). Deconvolution (Figure S10, Supporting Information) of the final spectrum showed that the band at 423 nm was still present, which suggests that part of the original diaqua-Ru_2 species is still present in solution. A plot of k_{obs} (see Table S5, Supporting Information) versus the histidine concentration for the fast reaction showed a square concentration dependence (Figure 8b) with a very small intercept. This behavior can be accounted for in terms of reactions 17 and 18, where his represents $(H_3N_2C_3)CH_2CH(NH_3^+)COO^-$, which are similar to reactions 11 and 12 for the reaction with cysteine. The rate law is given in (19) for which $K_1k_2 = (2.5 \pm 0.1) \times 10^3$ L^2 mol^{-2} s^{-1}and $k_{-2} = (2.86 \pm 0.01) \times 10^{-4}$ s^{-1} from Figure 8b.

$$[Ru_2(O_2CCH_3)_4(H_2O)_2]^+ + \text{his} \underset{k_{-1}}{\overset{k_1}{\rightleftharpoons}} [Ru_2(O_2CCH_3)_4(H_2O)(\text{his})]^+ + H_2O \quad (17)$$

$$[Ru_2(O_2CCH_3)_4(H_2O)(\text{his})]^+ + \text{his} \underset{k_{-2}}{\overset{k_2}{\rightleftharpoons}} [Ru_2(CH_3COO)_4(\text{his})_2]^+ + H_2O \quad (18)$$

$$k_{obs} = K_1k_2[\text{his}]^2 + k_{-2} \quad (19)$$

The second observed reaction step shows a linear dependence of k_{obs} (see Table S6, Supporting Information) on the histidine concentration without a meaningful intercept, which can be expressed by eq 20, for which $k_3 = 4.7 \pm 0.1$ L^{-1} mol^{-1} s^{-1} based on the plot in Figure 8c. This reaction step is ascribed to a subsequent decomposition reaction in which histidine displaces one of the bridging acetate groups.

$$k_{obs} = k_3[\text{his}] \quad (20)$$

Histidine also has three possible binding sites for metal ions: the carboxylate (COO), the amine (NH_2), and the imidazole ($H_3N_2C_3$) groups. The pK_a values of these groups are 1.70, 9.09, and 6.04,[38] respectively. Since the nitrogen atom of the imidazole ring is a strong donor, the imidazole group is the most probable site for coordination to ruthenium. Moreover, the pK_a value of this group is very close to pH 5.0 and it is probably fully deprotonated in the reaction medium. The fast reaction might be attributed to the substitution of the two coordinated water molecules by histidine via the imidazole ring. The slow reaction that shows a linear concentration dependence can be attributed to the substitution of one acetate group by his.

On the basis of the data summarized in Table 2, some trends for the reaction of tetrakis(acetato)ruthenium(II,III) with the amino acids can be observed. The first reaction of the diruthenium(II,III) paddlewheel framework with the four amino acids is reversible and involves axial substitution of one water molecule by the amino acid. The data suggest that the coordination of the amino acid to ruthenium occurs via the carboxylate group, which is also consistent with the fact that this group is deprotonated at pH 5.0 in contrast to the amino group. However, spectral evidence show that the reaction with amino acids is accompanied by the appearance of a new band in the visible at ~540 nm that could be better assigned to a chromophore having a Ru–N bond than a Ru–O bond. The reaction with glycine shows a decrease in pH in nonbuffered solution, and since the pK_a of the amino group will decrease once it binds to the metal center, we suggest that the first reaction may be followed by a fast intramolecular linkage isomerization from CO**O**– to –**N**H_2. A similar CO**O**– to –**N**H_2 isomerization may also occur in the reaction with tryptophan. In contrast, the reaction with cysteine may involve an intramolecular linkage isomerization from CO**O**– to –**S** due to the presence of the stronger donor thiol group in this amino acid. This behavior might be supported by the values of the rate constants k_1 and k_{-1} for axial substitution involving water and amino acid exchange in the diruthenium(II,III) paddlewheel framework that follows the relative order: cys ≫ trp ~ gly. The indole group of tryptophan seems to not have a significant

dx.doi.org/10.1021/ic300168t | Inorg. Chem. 2012, 51, 6615–6625

effect since the rate of the reaction is only 2.5 times higher than that found for glycine. The kinetics of the reaction with cysteine is about 10^5 times faster than the reaction with glycine, which indicates that the thiol group of cysteine plays an important role in the reaction. In the reaction with histidine, the nitrogen atom of the imidazole ring is the most probable site for coordination to ruthenium. It is also important to mention that in all cases, a significant amount of the starting diaqua-Ru_2 species still remains in solution.

Little is presently known about the intimate nature of the axial ligand displacement process. This is mainly due to the fact that no thermal and pressure activation parameters are presently available for the studied reactions. Our results show that the reactions with the studied amino acids are significantly slower than the reaction with chloride, but this could be partially due to the different concentration range employed in the latter system. It is claimed in the literature that the reactions of PCy_3 and $PPhCy_2$ with $[Ru_2(O_2CCH_3)_4(MeCN)_2]^+$ in MeCN to form mono- and diphosphane complexes, follow a dissociative substitution mechanism that is controlled by the release MeCN.[39] The authors observed a linear dependence of the observed first-order rate constants on the phosphane concentration for the first reaction step, from which overall second-order rate constants could be reported. The latter turned out to be very similar for the different phosphanes studied, which the authors interpreted as evidence for a dissociative mechanism.[39] This conclusion is quite logical and may indeed be correct, but it should be kept in mind that in terms of a dissociative mechanism, the second order rate constant is a composite value of rate constants for the release and binding of MeCN, and for the binding of the phosphane to the coordinatively unsaturated intermediate. As a result, the interpretation of the rate constants and the corresponding thermal activation parameters becomes more complex.

CONCLUSIONS

In this report we have studied the thermodynamics of axial ligand substitution reactions and the kinetic reactivity toward amino acids for the tetrakis(acetato)chloridodiruthenium(II,III) complex. The dissolution of the paddlewheel $[Ru_2(CH_3COO)_4Cl]$ complex in water leads mainly to the formation of the axially substituted diaqua-Ru_2 species. Starting from these species we could follow the two successive water/chloride equilibration reactions. Calculations of thermodynamic standard reaction parameters ΔH°, ΔS°, and ΔV° showed that both the sequential axial substitution reactions of water by chloride are thermodynamically favorable and are enthalpy driven. Both these reactions are fast in the presence of the large excess of chloride required to form the chlorido complexes and their kinetics could not be studied under these conditions. The kinetic behavior of the tetrakis(acetato)diruthenium(II,III) complex toward amino acids showed that the axial substitution of the first water molecule by amino acids follows the relative order cys $\gg$ trp $\sim$ gly. The thiol and imidazole groups of the amino acids cysteine and histidine, respectively, have important effects on the axial substitution kinetics. Coordination of the amino acids to ruthenium occurs via the axial position to form aqua(amino acid)-Ru_2 substituted species. However, deconvolution of the final spectra showed that a significant amount of the starting diaqua-Ru_2 species still remains in solution. The results revealed evidence that the $[Ru_2(RCOO)_4]^+$ paddlewheel framework is mostly maintained in the presence of the amino acids. These studies are relevant to elucidate the interactions in a physiological environment that might involve both water/chloride exchange and reactions with relevant bioligands such as amino acids. Further work is underway in our laboratory to evaluate similar reactions for $[Ru_2(d\text{NSAID})_4Cl]$ metallo drugs.

ASSOCIATED CONTENT

Supporting Information

Plots of $RT \ln K$ vs $1/T$ and $RT \ln K$ vs P for diaqua-Ru_2 in the presence of excess chloride. Absorption spectra for selected steps of reactions between the diaqua-Ru_2 complex and amino acids and their correspondent kinetic traces (glycine, in the time range 1−10 h; cysteine, in the time ranges 1−30 s and 40−500 s). Kinetic traces for the reaction of diaqua-Ru_2 with the amino acids tryptophan (525 nm) and histidine (545 nm). Deconvolution of the absorption spectrum for selected steps of reactions between the diaqua-Ru_2 complex and amino acids (glycine, first and second steps; cysteine, first step; tryptophan, first step; histidine, first step). Tables of the observed rate constants (k_{obs}) obtained from the kinetic traces for the reactions between the diaqua-Ru_2 complex and amino acids at different concentrations (glycine, first step; cysteine, first and second steps; tryptophan, first step; histidine, first and second steps). This material is available free of charge via the Internet at http://pubs.acs.org.

AUTHOR INFORMATION

Corresponding Author

*E-mail: deosilva@iq.usp.br (D.d.O.S.); vaneldik@chemie.uni-erlangen.de (R.v.E.).

Notes

The authors declare no competing financial interest.

ACKNOWLEDGMENTS

The authors gratefully acknowledge the financial support from Brazilian agencies: Fundação de Amparo à Pesquisa de São Paulo (FAPESP) and Conselho Nacional de Desenvolvimento Científico e Tecnológico (CNPq). We are thankful for scholarships to R.L.S.R.S., from Coordenação de Aperfeiçoamento de Pessoal de Nível Superior (CAPES), for Ph.D. in Brazil, and CAPES/CNPq/Deutscher Akademischer Austausch Dienst (DAAD), for a four-month sandwich stay in Germany. The authors also acknowledge contributions from A. L. Barros (Brazil) and Dr. Erika Ember (Germany) for experimental and technical support.

REFERENCES

(1) Cotton, F. A., Murillo, C. A., Walton., R. A., Eds. *Multiple bonds between metal atoms*, 3rd ed.; Springer Science and Business Media, Inc.: New York, USA, 2005.

(2) Stephenson, T. A.; Wilkinson, G. *J. Inorg. Nucl. Chem.* **1966**, *28*, 2285−2291.

(3) Bennet, M. J.; Caulton, K. G.; Cotton, F. A. *Inorg. Chem.* **1969**, *8*, 1−6.

(4) (a) Clark, R. J. H.; Franks, M. L. *J. Chem. Soc., Dalton Trans.* **1976**, *18*, 1825−1828. (b) Norman, J. G., Jr.; Renzoni, G. E.; Case, D. A. *J. Am. Chem. Soc.* **1979**, *101*, 5256−5267.

(5) (a) Aquino, M. A. S. *Coord. Chem. Rev.* **1998**, *170*, 141−202. (b) Aquino, M. A. S. *Coord. Chem. Rev.* **2004**, *248*, 1025−1045.

(6) (a) Keppler, B. K., Ed. *Metal Complexes in Cancer Chemotherapy*; Wiley VCH: New York, USA, 1993. (b) van Rensburg, C. E. J.; Kreft, E.; Swarts, J. C.; Dalrymple, S. R.; Macdonald, D. M.; Cooke, M. W.; Aquino, M. A. S. *Anticancer Res.* **2002**, *22*, 889−892.

(7) de Oliveira Silva, D. *Anti Canc. Agents Med.Chem.* **2010**, *10*, 312−323.

(8) Ribeiro, G.; Vichi, F. M.; de Oliveira Silva, D. *J. Mol. Struct.* **2008**, *890*, 209−214.
(9) (a) Mori, W.; Sato, T.; Kato, C. N.; Takel, T.; Ohmura, T. *Chem. Rec.* **2005**, *5*, 336−351. (b) Kato, C. N.; Ono, M.; Hino, T.; Ohmura, T.; Mori, W. *Catal. Commun.* **2006**, *7*, 673−677. (c) Kato, C. N.; Mori, W. *C. R. Chim.* **2007**, *10*, 284−294. (d) Kataoka, Y.; Miyazakia, Y.; Satoa, K.; Saito, T.; Nakanishib, Y.; Kiatagwa, Y.; Kawakami, T.; Okumura, M.; Yamaguchi, K.; Mori, W. *Supramol. Chem.* **2011**, *23*, 287−296.
(10) Barker, J. E.; Ren, T. *Inorg. Chem.* **2008**, *47*, 2264−2266.
(11) Barral, M. C.; González-Pietro, R.; Herreo, S.; Jiménez-Aparício, R.; Priego, J. L.; Royer, E. C.; Torres, M. R.; Urbanos, F. A.; Zamora, F. *J. Clust. Sci.* **2008**, *19*, 219−230.
(12) (a) Chaia, Z. D.; Rusjan, M. C.; Castro, M. A.; Donnio, B.; Heinrich, B.; Guillon, D.; Baggio, R. F.; Cukiernik, F. D. *J. Mater. Chem.* **2009**, *19*, 4981−4991. (b) Chaia, Z.; Zelcer, A.; Donnio, B.; Rusjan, M.; Cukiernik, F. D.; Giroud-Godquin, A. M. *Liq. Cryst.* **2004**, *31*, 1019−1025.
(13) Mikuriya, M.; Yoshioka, D.; Borta, A.; Luneau, D.; Matoga, D.; Szklarzewiczc, J.; Handa, M. *New J. Chem.* **2011**, *35*, 1226−1233.
(14) (a) Ren, T. *Organometallics* **2005**, *24*, 4854−4870. (b) Xi, B.; Ren, T. *C. R. Chim.* **2009**, *12*, 321−331.
(15) Drysdale, K. D.; Beck, E. J.; Cameron, T. S.; Robertson, K. N.; Aquino, M. A. S. *Inorg. Chim. Acta* **1997**, *256*, 243−252.
(16) Vamvounis, G.; Caplan, J. F.; Cameron, T. S.; Robertson, K. N.; Aquino, M. A. S. *Inorg. Chim. Acta* **2000**, *304*, 87−98.
(17) Cooke, M. W.; Murphy, C. A.; Cameron, T. S.; Beck, E. J.; Vamvounis, G.; Aquino, M. A. S. *Polyhedron* **2002**, *21*, 1235−1244.
(18) Gilfoy, H. J.; Robertson, K. N.; Cameron, T. S.; Aquino, M. A. S. *Inorg. Chim. Acta* **2002**, *331*, 330−335.
(19) Andrade, A.; Namora, S. F.; Woisky, R. G.; Wiezel, G.; Najjar, R.; Sertie, J. A. A.; de Oliveira Silva, D. *J. Inorg. Biochem.* **2000**, *81*, 23−27.
(20) Ribeiro, G.; Benadiba, M.; Colquhoun, A.; de Oliveira Silva, D. *Polyhedron* **2008**, *27*, 1131−1137.
(21) Benadiba, M.; Santos, R. R. P.; de Oliveira Silva, D.; Colquhoun, A. *J. Inorg. Biochem.* **2010**, *104*, 928−935.
(22) Ribeiro, G.; Benadiba, M.; de Oliveira Silva, D.; Colquhoun, A. *Cell Biochem. Funct.* **2010**, *28*, 15−23.
(23) Jones, C. J.; Thornback, J. R. *Medicinal Applications of Coordination Chemistry*; The Royal Society of Chemistry: Cambridge, UK, 2007.
(24) Gianferrara, T.; Bratsos, I.; Alessio, E. *Dalton Trans.* **2009**, *37*, 7588−7598.
(25) Lippert, B. *Cisplatin: Chemistry and Biochemistry of a Leading Anticancer Drug*; Wiley-VCH: Zürich, Switzerland, 1999.
(26) Chifotides, H. T.; Dunbar, K. R. *Acc. Chem. Res.* **2005**, *38*, 146−156.
(27) Timerbaev, A. R.; Hartinger, C. G.; Aleksenko, S. S.; Keppler, B. K. *Chem. Rev.* **2006**, *106*, 2224−2248.
(28) Jakupec, M. A.; Galanski, M.; Arion, V. B.; Hartinger, C. G.; Keppler, B. K. *Dalton Trans.* **2008**, *2*, 183−194.
(29) Hartinger, C. G.; Jakupeca, M. A.; Zorbas-Seifrieda, S.; Groessla, M.; Eggera, A.; Bergerd, W.; Zorbasc, H.; Dyson, P. J.; Keppler, B. K. *Chem. Biodivers.* **2008**, *5*, 2140−2155.
(30) Ang, W. H.; Daldini, E.; Juillerat-Jeanneret, L.; Dyson, P. J. *Inorg. Chem.* **2007**, *46*, 9048−9050.
(31) Hartinger, C. G.; Zorbas-Seifried, S.; Jakupec, M. A.; Kynast, B.; Zorbas, H.; Keppler, B. K. *J. Inorg. Biochem.* **2006**, *100*, 891−904.
(32) Mitchell, R. W.; Spencer, A.; Wilkinson, G. *J. Chem. Soc., Dalton Trans.* **1973**, *8*, 846−854.
(33) Schmeisser, M.; van Eldik, R. *Inorg. Chem.* **2009**, *48*, 7466−7475.
(34) (a) Spitzer, M.; Gartig, F.; van Eldik, R. *Rev. Sci. Instrum.* **1988**, *59*, 2092−2093. (b) le Noble, W. J.; Schlott, R. *Rev. Sci. Instrum.* **1976**, *47*, 770−772.
(35) (a) Martin, D. S.; Newman, R. A.; Vlasnik, L. M. *Inorg. Chem.* **1980**, *19*, 3404−3407. (b) Clark, R.; Ferris, R. L. *Inorg. Chem.* **1981**, *20*, 2759−2766. (c) Miskowski, V. M.; Loehr, T. M.; Gray, H. B. *Inorg. Chem.* **1987**, *26*, 1098−1108. (d) Miskowski, V. M.; Gray, H. B. *Inorg. Chem.* **1988**, *27*, 2501−2506. (e) Estiú, G.; Cukiernik, F. D.; Maldivi, P.; Poizat, O. *Inorg. Chem.* **1999**, *38*, 3030−3039.
(36) Castro, M. A.; Roitberg, A. E.; Cukiernik, F. D. *Inorg. Chem.* **2008**, *47*, 4682−4690.
(37) Dema, A. C.; Bose, R. N. *Inorg. Chem.* **1989**, *28*, 2711−2713.
(38) Lide, D. R., Ed. *CRC Handbook of Chemistry and Physics*, 90th ed.; CRC Press/Taylor and Francis: Boca Raton, FL, 2010.
(39) Burchell, T. J.; Cameron, T. S.; Macartney, D. H.; Thompson, L. K.; Aquino, M. A. S. *Eur. J. Inorg. Chem.* **2007**, 4021−4027.